Application of a simple DNA damage model developed for electrons to proton irradiation

Yusuke Matsuya[1*], Takeshi Kai[1], Alessio Parisi[2,3], Yuji Yoshii[4] and Tatsuhiko Sato[1]

[1] *Nuclear Science and Engineering Center, Japan Atomic Energy Agency, Tokai, Ibaraki, Japan*
[2] *Radiation Protection Dosimetry and Calibration Expert Group, Belgian Nuclear Research Centre, Mol, Belgium*
[3] *Department of Radiation Oncology, Mayo Clinic, Jacksonville, Florida, USA*
[4] *Central Institute of Isotope Science, Hokkaido University, Sapporo, Hokkaido, Japan*
*Corresponding author: matsuya.yusuke@jaea.go.jp (Yusuke Matsuya)

ABSTRACT

Proton beam therapy allows irradiating tumor volumes with reduced side effects on normal tissues with respect to conventional X-ray radiotherapy. Biological effects such as cell killing after proton beam irradiations depend on the proton kinetic energy, which is intrinsically related to early DNA damage induction. As such, DNA damage estimation based on Monte Carlo simulations is a research topic of worldwide interest. Such simulation is a mean of investigating the mechanisms of DNA strand break formations. However, past modellings considering chemical processes and DNA structures require long calculation times. Particle and Heavy Ion Transport System (PHITS) is one of the general-purpose Monte Carlo codes that can simulate track structure of protons, meanwhile cannot handle radical dynamics simulation in liquid water. It also includes a simple model enabling the efficient estimation of DNA damage yields only from the spatial distribution of ionizations and excitations without DNA geometry, which was originally developed for electron track-structure simulations. In this study, we investigated the potential application of the model to protons without any modification. The yields of single-strand breaks, double-strand breaks (DSBs) and the complex DSBs were assessed as functions of the proton kinetic energy. The PHITS-based estimation showed that the DSB yields increased as the linear energy transfer (LET) increased, and reproduced the experimental and simulated yields of various DNA damage types induced by protons with LET up to about 30 keV/μm. These results suggest that the current DNA damage model implemented in PHITS is sufficient for estimating DNA lesion yields induced after protons irradiation except at very low energies (below 1 MeV). This model contributes to evaluating early biological impacts in radiation therapy.

Keywords: DNA damage yields, Monte Carlo track-structure simulation, proton beams,

1. INTRODUCTION

Proton beam therapy (PBT), which has been widely installed in clinics, is one of the effective approaches to eliminate solid tumors by dose concentrations to a tumor at the Bragg

peak region (*1*,*2*). The biological impacts for PBT relative to photon beams (referred to as relative biological effectiveness [RBE]) is generally defined as 1.1 (*2*) because of the major contribution of secondary electrons (*3*) interacting with DNA (liquid water). However, it has been proposed that the use of a constant RBE = 1.1 for protons is no longer appropriate (*4*,*5*). Therefore, quantifying the variable RBE value depending on proton energy (i.e., the increase in RBE at the Bragg peak region) from the standpoints of radiation therapy and radiation biology is necessary.

When quantifying such RBE value of PBT, tumor cell killing is usually evaluated. Several reports show that cell death (such as apoptosis, necrosis, and autophagy (*6*)) is induced by radiation-induced DNA double-strand breaks (DSBs) with a certain probability (*7*-*10*). As such, the dependence of proton energy (as well as linear energy transfer [LET]) on DSB induction has been evaluated to date (*11*). There are several techniques for measuring DSB yields (e.g., immunofluorescent staining and agarose gel electrophoresis). (*12*-*15*). The DSB yields for any proton energies can be quantified using both plasmid DNA and cultured cell lines based on such experimental techniques. However, the yields for low-energy protons (i.e., < 1 MeV protons) can be obtained only by dry plasmid DNA (*16*) as low-energy protons have a correspondingly short range in water. For example, the ranges of 1 MeV and 300 keV protons are approximately 23.9 and 3.78 μm, respectively. When performing such experiments *in vitro*, the yields can vary depending on the experimental conditions, that is, cell shape (*17*) and plasmid condition (liquid or dry) (*18*). Therefore, grasping experimental geometry and the proton kinetics in the biomaterials is necessary for obtaining the relationship between proton energy and DNA damage yields.

Monte Carlo simulations are an efficient approach to mechanistically investigate the relationship between proton energy (as well as LET) and DNA damage yields. In particular, track-structure simulation at the DNA level (nanometer scale) in liquid water (*19*-*21*) enables mechanistically estimating DNA damage yields and types (i.e., single-strand breaks [SSBs], DSBs, and complex DSBs) (*22*-*25*) even for low-energy protons (i.e., < 1 MeV protons). The past modellings for estimating DNA damage yields have considered chemical processes (free radicals) and DNA structures in detail (*26*,*27*). However, the past modellings which consider chemical processes and DNA structure need a long calculation time. Recently, DNA damage estimation is getting more and more attention in the field of medical physics (*28*,*29*). In order to reduce computing time, simplified models of evaluating DNA damage induction are of interest. However, at the price of computing time reduction, these simplified models can only simulate the physical stage of radiation interaction and do not model radical diffusion nor chemical reactions. With reasonable short computing time, estimating DNA damage yields with high precision is therefore of great importance as mechanism study.

Several similar approaches, such as density-based spatial clustering of applications with noise (DBSCAN) (*30*) and ion cluster size distribution (*31*) have been proposed. However, by focusing on only the number and the distance of the events (ionizations and excitations), we

developed a simple model for efficiently estimating DNA damage yields (*32*-*34*) by the track-structure mode in the Particle and Heavy Ion Transport System (PHITS) (*35*-*37*). This model enables efficiently estimating DNA damage types and yields only using spatial distribution of ionizations and excitations where track-structure mode is activated. In addition, in the recent PHITS development, the physical models of Kyushu University Radiobiology Unit Code (KURBUC) of protons and Carbon ions was implemented in PHITS under the name of *PHITS-KURBUC* mode, which enables simulating atomic interactions (i.e., elastic scattering, ionization, excitation, dissociative electron attachment, vibrational excitation, photon excitation, rotational excitation, electron capture, and electron loss) of protons in liquid water (*36*). Meanwhile, the current PHITS code does not explicitly simulate radical diffusion and chemical reactions to DNA. To date, the DNA damage model in PHITS has been verified only for electron (as well as photon) irradiation (*32*-*34*). The estimation of DNA damage yields for proton irradiation is in principle possible with the PHITS code but has not been investigated yet.

In this study, applying the simplified model to proton irradiation, we evaluated the yields of SSBs, DSBs, and complex DSBs for proton beams, and compared them with the corresponding experimental data and other simulation results. From the comprehensive comparisons, we discussed the effectiveness of the current DNA damage estimation model based on the PHITS track-structure simulation mode in the case of proton beam irradiations. Throughout this evaluation, we show the simple DNA damage estimation model implemented in the PHITS code would contribute to understanding early biological impacts in PBT.

2. MATERIALS AND METHODS

2-1. Simulation setup and physical processes

We used PHITS ver. 3.27 (*35*) and simulated electron and proton tracks using two model types: one is the condensed-history method for the macroscopic scale and the other is the track-structure mode for the microscopic scale (DNA scale). For the condensed-history method, the ATIMA mode (*38*) and the electron gamma shower (EGS) mode (*39*) were used, and the transport cut-off energies were set to 1 keV for both electrons and protons. For the track-structure simulations, the electron track-structure mode (*etsmode*) (*32*) and the proton track-structure *PHITS-KURBUC* mode (*36*) were used to simulate atomic interactions along proton track in the region where the track-structure section is activated. In the track-structure simulations, the cut-off energies for transporting electrons and protons were 1 eV and 1 keV, respectively.

2-2. Estimation of SSB and DSB yields

The simple geometry composed of three cuboids illustrated in Fig. 1A was considered for estimating proton-induced DNA damage yields. In this geometry, the track-structure mode was activated in the central region (REG2), while the condensed history approach was taken in

REG1 and REG3. Examples of simulated proton tracks are depicted in Fig. 1B, where 10 tracks of 100, 10 and 1 MeV protons were simulated. The thickness of REG2 was defined to be large enough that at least 1% of the proton energy is being deposited in this region. For example, for 1 MeV protons a thickness of 382 nm is needed. For higher energies, larger thicknesses would be needed, however, this would result in long computing times. Hence, for proton energies larger than 1 MeV, a constant thickness of 1 μm was chosen. Meanwhile, judged from radial dose distribution, secondary electrons deposit their energy and almost stop within 100 nm from proton track (*34*). Considering this, 100 nm was chosen as the thicknesses of REG1 and REG3. Using this geometry, we simulated the proton tracks and spatial coordinates of the atomic interactions based on the *PHITS-KURBUC mode*. Note that the δ-rays coming into REG2 from REG1 and REG3 were considered to establish the secondary electron equilibrium.

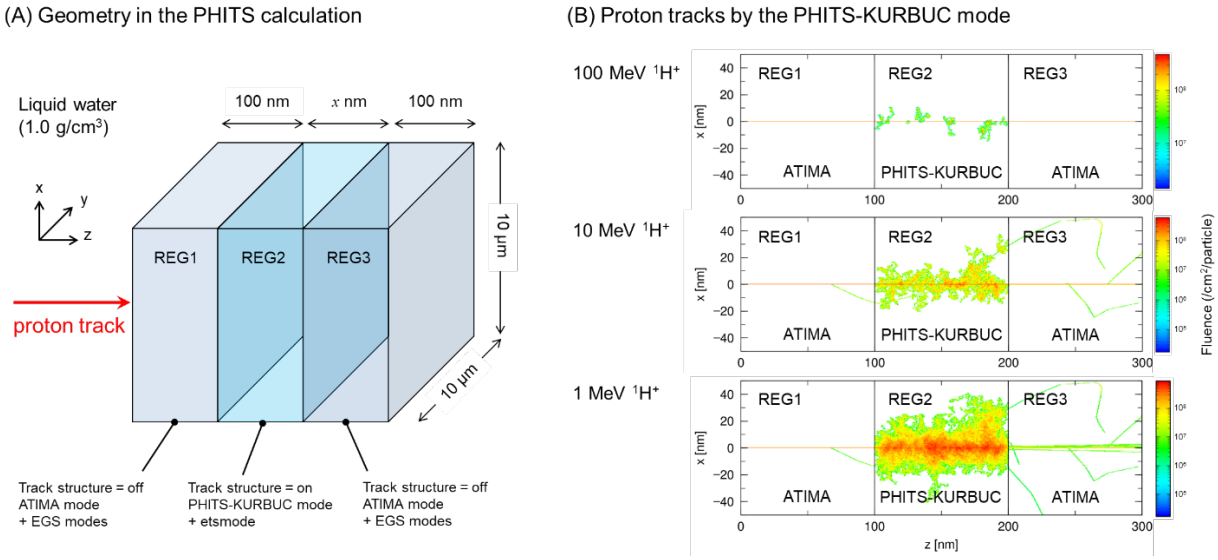

Figure 1. Simulation geometry and proton track structure in PHITS: (A) is the geometry for estimating DNA damage yields, and (B) is the generated 10 proton tracks at 100, 10, and 1 MeV. The track-structure modes are turned on only in REG2. The cut-off energies for electrons and protons are set to 1.0 eV and 1.0 keV, respectively. In Fig. 1B, proton tracks were depicted using the constant thickness of REG2 (= 100 nm) as examples. When estimating the yields of DNA damage, the thickness of REG2 was defined to be large enough that at least 1% of the proton energy is being deposited in this region. Note that for proton energies larger than 1 MeV, a constant thickness of 1 μm was chosen.

Assuming that the number of the events (i.e., ionizations and excitations) per deposited energy N_{event}/E_{dep} and that of linkage composed of two events within 10 bp (3.4 nm) per deposited energy N_{link}/E_{dep} are proportional to the yields of strand breaks (SBs) and DSBs, the yields SBs and DSBs (Y_{SB} and Y_{DSB}) can be calculated as follows (*36*):

$$Y_{SB} = k_{SB} \frac{N_{event}}{E_{dep}}, \qquad (1)$$

$$Y_{DSB} = k_{DSB} \frac{N_{link}}{E_{dep}}, \quad (2)$$

where k_{SB} and k_{DSB} are the coefficients for estimating the yields of SBs and DSB from the events and the linkages, respectively (keV/Gy/Da). These coefficients can be determined by fitting the experimental yields of SSB and DSB after exposure to photon beams (i.e., 220 kVp X-rays) as reported previously (*32*). Induction of indirect DNA damage by radical species, such as OH radicals, are implicitly considered in these coefficients, although the kinematics of the radicals are not explicitly reproduced in the model. The DBSCAN, which is similar as this model, is known as a simple approach which can obtain the SSB and DSB yields from events per cluster (*30*). Unlike the algorithms of DBSCAN, the present model focuses on only scoring the number of events and distance between two events (*32*). This model does not need to classify the cluster and noise from spatial distributions of atomic interactions, which is expected to reduce computational time. It should be noted that the implicit consideration of chemical reactions in this model has some drawbacks, i.e., the influence of LET is not accounted for explicitly.

Because of the update of *etsmode* for electron kinetic energy higher than 100 keV in the latest PHITS ver. 3.27, we redetermined these coefficients so as to reproduce the experimental yields of SSB and DSB after 220-kVp X-rays exposure (*40*,*41*) (here, k_{SB} = 6.46 × 10^{-12} keV $Gy^{-1}Da^{-1}$, k_{DSB} = 1.48 × 10^{-13} keV $Gy^{-1}Da^{-1}$). The benchmark test for the model performance was remade for monoenergetic electrons (Fig. S1) and for photon beams (Fig. S2A), where we confirmed that the yields of electron-induced SSB and DSB estimated using the updated parameters showed the same results as those reported previously (*32*). Note that the yield of SSBs, Y_{SSB}, can be obtained by subtracting 2 × Y_{DSB} from Y_{SB}. Using this simplified DNA damage estimation model with the updated parameters, we calculated the Y_{SSB} and Y_{DSB} for various proton kinetic energies. The number of simulated particles was adapted to reach a statistical uncertainty of less than 1%. The estimated DSB yields were compared with other simulation results (i.e., Geant4-DNA, original KURBUC and PARTRAC) (*30*,*42*,*43*) and the corresponding experimental data (using cultured cells and plasmid DNA) (*30*,*44*-*46*) in the literature. The detail of the comparative data is summarized in Table S1.

2-3. Estimation of DSB complexity

Assuming that the number of events (i.e., ionizations and excitations) is proportional to the yield of SB, we also classified the DSB complexity from a simplified cluster analysis using the number of events within a 10-bp (3.4 nm) diameter at a DSB site (a gravity of linkage), N_{cl} (*33*). We deduced that 12 events were needed on average to induce an additional SB at a DSB site to reproduce the experimental complex DSB measured by atomic force microscopy (*33*). In the same manner as that for the model for estimating SSB and DSB yields, we updated the criteria for determining complex DSB, i.e., DSB+ (a DSB coupled with an SB) and DSB++ (a DSB coupled with two SBs). The number of ionization and excitations at a DSB site (i.e., a

sphere with a 3.4-nm radius) increased by about 1% because of the update of *etsmode* by the recent PHITS development. Therefore, when estimating the DSB complexity, we used the following criteria: simple DSB (sDSB) for $2 \leq N_{cl} \leq 14$, DSB+ for $14 < N_{cl} \leq 26$ and DSB++ for $N_{cl} > 26$. The benchmark results for this update are summarized in Fig. S2B, where it is also confirmed that the updated parameters enabled the estimation of a similar tendency as reported previously (*34*). Using the same geometry illustrated in Fig. 1A and this simplified model, we estimated the contents of DSB+ and DSB++ for 10 keV electrons, 30 MeV protons, 2 MeV protons and 1 MeV protons and compared them with the simulation data calculated by the original KURBUC (*42*) and Geant4-DNA (*47*). In the same manner as that for the DSB yields, DSB complexity was calculated with sufficient numbers of particles to make the statistical uncertainty less than 1%.

2-4. RBE values for early SSB and DSB induction

The RBE values for SSB and DSB, referred to as RBE_{SSB} and RBE_{DSB}, respectively, were calculated using the *PHITS-KURBUC mode*. We selected 200 kVp X-rays (0.5-mm Al + 0.5-mm Cu filtration) as the reference radiation throughout this study. This kind of 200 kVp X-rays with such filtration is often used in the field of radiation biology. The DNA damage yields immediately after irradiation are proportional to the absorbed dose (*48*,*49*). Regarding this, the RBE_{SSB} and RBE_{DSB} were calculated using the following equations.

$$RBE_{SSB} = \frac{Y_{SSB}}{Y_{SSB(200\text{-kVp X-rays})}}, \quad (3)$$

$$RBE_{DSB} = \frac{Y_{DSB}}{Y_{DSB(200\text{-kVp X-rays})}}, \quad (4)$$

where Y_{SSB} and Y_{DSB} are the SSB and DSB yields for any radiation, respectively; $Y_{SSB(200\text{-kVp X-rays})}$ and $Y_{DSB(200\text{-kVp X-rays})}$ are the SSB and DSB yields for the 200 kVp X-rays. The estimated yields of Y_{SSB} and Y_{DSB} as a function of LET were compared with the available experimental data (*16*,*18*,*30*,*44*-*46*,*53*-*56*,*58*) and the other simulation data (*42*,*43*,*47*,*50*-*52*). The data list used for this comparison is summarized in Table S1. It should be noted that the simulation data by the MCMS algorithm was calculated in this study (*51*,*52*). From the comparison, we evaluated the RBE values for DNA damage induced by proton beams.

The LET values are also calculated to investigate the relationship between LET and RBE for DSB (RBE_{DSB}). Figure 2 shows the relations between proton kinetic energy and stopping power (LET) for the *PHITS-KURBUC mode*, which were compared with the recommended data of the International Commission on Radiation Units and Measurements (ICRU) Report 49 (*60*), other simulations (*61*-*63*), and the PHITS condensed-history mode of ATIMA. It should be noted that the LET for ATIMA mode was obtained by the t-LET tally, which can provide information on track length and dose as a function of the LET of a given material. As shown in Fig. 2, it was confirmed that the stopping power (LET) of the *PHITS-KURBUC mode* agrees

well with that of the condensed-history ATIMA mode and the ICRU Report 49 (*60*).

We also compared the RBE_{DSB} estimated by PHITS with the experimental RBE_{DSB} using proton energy as a parameter to evaluate the accuracy of the PHITS simulation. We recalculated the DSB yields by γ-rays (^{60}Co and ^{137}Cs sources), kVp X-rays (30–250 kVp), ultra-soft X-rays (Ti_K, Al_K, Cu_L, and C_K), monoenergetic electrons and monoenergetic protons on the basis of the current DNA damage model. For the simulation for monoenergetic electrons, we simulated whole electron tracks using *etsmode*. When calculating the yields of photon beams, γ-rays and kVp X-rays were incident to a water cuboid ($10 \times 10 \times 0.1$ cm^3) surrounded by air as shown in Fig. S3. The track-structure mode was activated in liquid water (REG2 in Fig. S3), while the condensed-history approach was taken in air (REG1 in Fig. S3). For the monoenergetic protons, the particles were incident to liquid water, as shown in Fig. 1. Note that the simulation setup is the same as that for the simulation for monoenergetic protons used in Fig. 1. The PHITS results were compared with the experimental data (*16*,*18*,*30*,*44*-*46*,*53*-*56*,*58*). The RBE_{DSB} was calculated using 200 kVp X-rays as reference radiation.

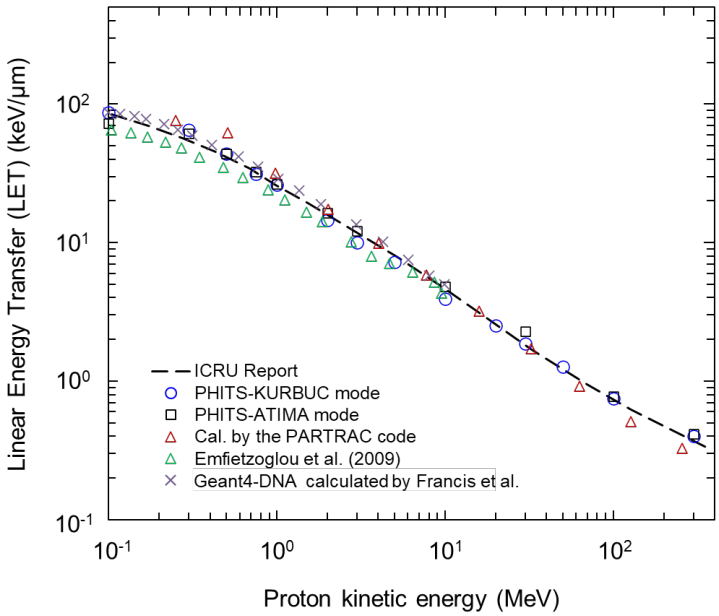

Figure 2. LET value as a function of proton kinetic energy. The *PHITS-KURBUC mode* (open blue circle) results are compared with the recommended data of ICRU Report 49 (*60*), other simulations (*61*-*63*), and the PHITS condensed-history mode of ATIMA. Note that the LET for the ATIMA mode is obtained by the t-LET tally.

2-5. Measurement of the cross-sections of cell nuclei

We measured the cross-section of cell nuclei of various cell lines in this study to grasp the experimental condition using cultured cells. We used five types of cell lines: Chinese Hamster fibroblast cell line V79-379A (IFO50082, JCRB Cell Bank, Japan), human lung fibroblast cell line WI-38 (RCB0702, RIKEN, Japan), human lung bronchial epithelial cell line HBE3-KT (CRL-4051, ATCC, Manassas, VA, USA), human prostate cancer (DU145), and non-small cell lung cancer A549 (RCB3677, RIKEN Cell Bank, Japan). The V79-379A cells were

maintained routinely in Dulbecco's modified Eagle's medium (DMEM) (D0819, Sigma Life Science) supplemented with 10% fetal bovine serum (FBS) and 1% penicillin/streptomycin (p/s) (Sigma Life Science). The WI-38 cells and the A549 cells were maintained in the DMEM/Nutrient Mixture F-12 (DMEM/F12) (D8437, Sigma Life Science) supplemented with 10% FBS (FBS, Equitech-Bio Inc.) and 1% p/s. The HBEC3-KT cells were maintained in a bronchial epithelial cell medium (3211NZ, ScienCell). DU145 cells were grown in RPMI-1640 with L-glutamine (Thermo Fisher Scientific Inc.) supplemented with 10% FBS (FBS, Equitech-Bio Inc.) and 1% p/s. All cells were maintained at 37°C in a humidified atmosphere of 95% air/5% CO_2.

All cells were fixed in 4% paraformaldehyde for 10 min on ice and were then permeabilized in 0.2% v/v Triton X-100 in phosphate-buffered saline (PBS) for 5 min. After rinsing with PBS, the cells were incubated with 1 μg/ml DAPI solution (62248, Thermo Fisher Scientific) for 15 min. After rinsing with PBS, the cells were observed using a high standard all-in-one fluorescent microscope (BZ-9000; Keyence, Osaka, Japan). The sizes of the cell nuclei were measured using the ImageJ software (*64*). The microscopic images of stained cell nuclei and the histogram of the cross-sections are shown in Fig. S4A and Fig. S4B, respectively, (see supplementary material), from which we calculated the mean radii of the ellipsoidal section of the cell nuclei for all cell lines. Information on cell nucleus size was used for this DNA damage simulation.

2-6. DNA damage simulation for PBT considering cell geometry

Using the mean radii measured by DAPI staining, we estimated the cell geometry, as shown in Fig. S4A. The thickness of the cell cannot be measured by the microscopy used in this study because of the spatial resolution of the z-stack. Thus, we used the ratio between the mean radius of the ellipsoidal section of a cell nucleus and the thickness of the cell cytoplasm shown in the literature (*65*). The geometry of the cytoplasm was assumed as half of an ellipse with a constant 5-μm thickness. In this simulation, we used the cross-section of the lung fibroblast cell lines, i.e., V79-379A and WI-38. We also measured the cross-sections for a few additional cell lines (i.e., HBE3-KT, DU145 and A549). However, no relevant differences were observed among these cell lines (Fig. S4B).

For the DNA damage simulation for PBT, we first reproduced the monoenergetic 60 MeV proton beam line reported by Chaudhary et al (*58*). In reproducing percentage of depth dose (PDD) of the 60 MeV proton beams, we assumed a 0.8% standard deviation of the incident proton energy when accelerated. The proton beams were incident to a water cube ($40 \times 40 \times 40$ cm^3). We scored the energy spectra of proton beam at each depth to efficiently calculate the yields, and the protons were simulated using the spectra and the cell geometry (see Fig. S5). The thickness of the culture dish ($(C_8H_8)_n$, 1.00 g/cm^3) was set to 1 mm. The track-structure modes (i.e., *etsmode* and *PHITS-KURBUC*) were activated within the cell, whereas the ATIMA and EGS modes were used in the geometry except for the inside of the cell. The cut-off energies

of electrons were set to be 1 keV and 7 eV for the EGS mode and *etsmode*, respectively. Meanwhile, the proton cut-off energy was set to 1 keV. Using the simulation setup, we estimated the depth-dependence of the DSB yields, and compared the PHITS results with the experimental DSB yield measured by the 53BP1 focus formation assay in the literature (*58*).

3. RESULTS AND DISCUSSION

3-1. Energy-dependence of DNA damage yields

Figure 3 shows the DSB yields estimated by the *PHITS-KURBUC mode*, which were compared with other available simulations (*30*,*42*,*43*) and the experimental data (*30*,*44*-*46*). The LET dependencies of the yields of SSB and DSB estimated by the PHITS code are also shown in Fig. S6. The PHITS estimation was performed using the geometry shown in Fig. 1. We also calculated the DSB yields using the cell geometry where the thickness of track-structure region is more than 1 μm to check the impact of the secondary electron equilibrium (see Fig. S7A). The DSB yields for high-energy protons (e.g., 100 MeV protons) are expected to be reduced when the equilibrium is violated; however, we observed no significant reduction. From these preliminary results, the DNA damage yields can be estimated under the charged particle equilibrium using the simulation setup shown in Fig. 1. In Fig. 3, the experimental data used for this comparison are composed of *in vitro* experiments with fibroblast cell lines (such as V79 cell line) and with plasmid DNA. The estimation of the KURBUC and the PARTRAC codes consider the indirect DNA damage induction by chemical processes such as that of the hydroxyl radical (OH radical).

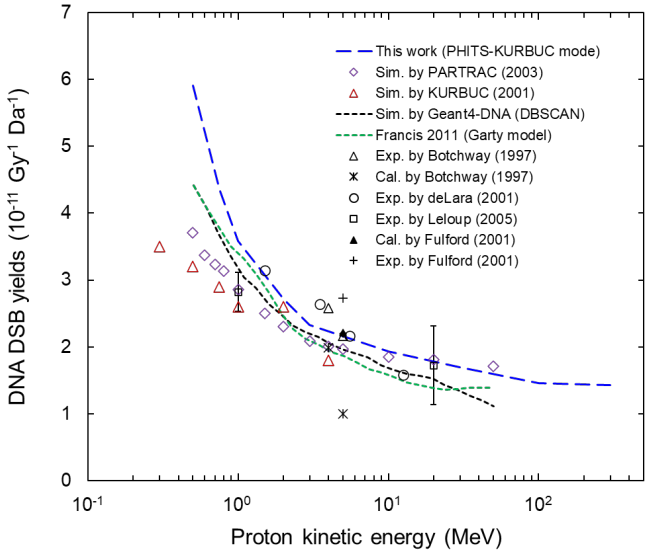

Figure 3. DSB yield in dependence on proton kinetic energy. The results of this work (blue dotted line) are estimated using the *PHITS-KURBUC* mode and the DNA damage estimation model. The PHITS estimation is compared with the available simulation data (*30*,*42*,*43*) and the experimental data (*30*,*44*-*46*). Note that the experimental data are composed of V79 cells (Botchway et al, 1997; deLara et al, 2001) and plasmid DNA (Fulford et al, 2001; Leloup et al, 2005). The experimental data by deLara are taken from Francis et al (2011) (*30*).

As shown in Figs. 3 and S5, the DSB yield increased as the proton kinetic energy decreased, and the PHITS estimation reasonably reproduced the experimental results (R^2 = 0.593). Meanwhile, focusing on protons with energies lower than 1 MeV, the DSB yields estimated by the PHITS code were higher than the published simulation results. However, there are no experimental results for monoenergetic protons with energies lower than 1 MeV. Thus, biomaterials have to be very thin, and the plasmid DNA under dry conditions must be suitable to obtain the experimental yields for such low-energy protons. Considering these, for the energy regime where experimental value measured in liquid water are available, the DNA damage estimation based on the simplified model is sufficient for reproducing the experimental DSBs.

On the other hand, the DSB yields for low-energy protons calculated by *PHITS-KURBUC mode* are higher than the corresponding data obtained from the other simulations considering chemical processes (KURBUC and PARTRAC) (*42*,*43*). This discrepancy is probably attributable to the fact that the coefficients for estimating the yields of SBs and DSB (k_{SB} and k_{DSB}) were determined to reproduce those of electron-induced DNA damage, i.e., our model intrinsically assumes that the ratios between radical recombination and indirect DNA damage induction are independent of the radiation type. This assumption may result in the inaccuracy in the DNA damage estimation for high LET radiation because the yields of OH radicals within a certain volume, which are related to the probabilities of radical recombination, increase with increasing LET. Therefore, further development of the model considering this LET dependence is desirable in future studies (*66*). However, because no experimental data are available for the DSB yields of protons with energies lower than 1 MeV, the accumulation of experimental data is also essential in the future.

3-2. LET dependence of RBE value for protons

We compared the RBE for SSB and DSB with the data available in the literature to further evaluate the yields of DNA damage estimated by the PHITS code. The PHITS simulation was performed using the geometry shown in Fig. 1. Figure 4A and 4B show the LET dependence of the RBE values estimated by the *PHITS-KURBUC mode* for SSB and DSB, respectively, where the PHITS estimation was compared with available experimental data (*16*,*18*,*30*,*44*-*46*,*53*-*56*,*58*) and other simulation data (*42*,*43*,*47*,*50*-*52*). Note that the reference radiation of the PHITS estimation was the 200-kVp X-rays with 0.5-mm Al and 0.5-mm Cu filtration (which is often used in cell experiments), whereas those for the data in the literature varied. The biological effects also depended on photon energy (*59*). Only a limited amount of the experimental RBE values, which are measured using specific photon energy (i.e., ^{60}Co γ-rays or 200 kVp X-rays), are available. For a precise comparison of the PHITS results and the experimental data, accumulating experimental data on DNA damage yields in the near future is necessary.

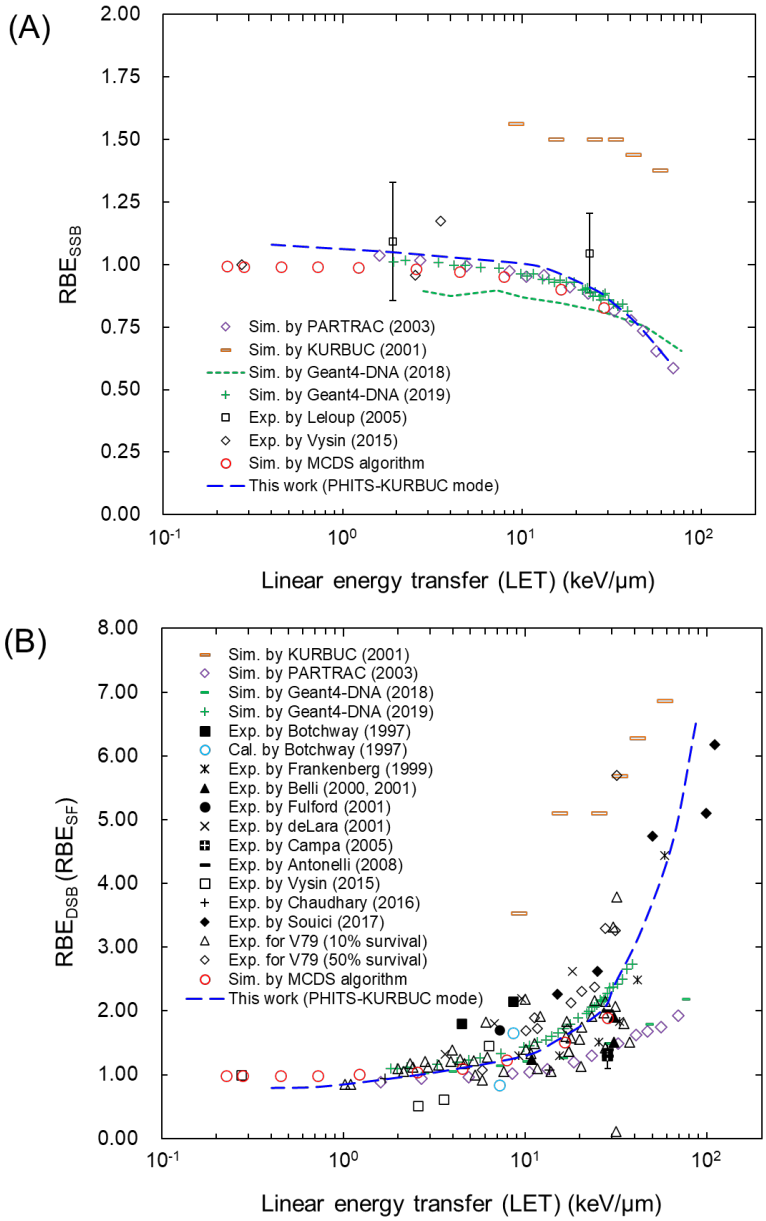

Figure 4. LET dependence on RBE values. (A) is the RBE for SSB and (B) is the RBE for DSB. The reference radiation of the PHITS estimation is the 200-kVp X-rays with 0.5-mm Al and 0.5-mm Cu filtration. The estimations by the PHITS code are compared with the available experimental data (*16*,*18*,*30*,*44*-*46*,*53*-*56*,*58*) and other simulation data (*42*,*43*,*47*,*50*-*52*).

In Fig. 4, RBE_{SSB} gradually decreased as the LET increased, whereas RBE_{DSB} gradually increased as the LET increases. Considering the large uncertainties of RBE values in the literature, the PHITS estimation reasonably agreed with the experimental and the other simulated data. Focusing on the high-LET region (i.e., greater than approximately 30 keV/μm), the RBE_{DSB} rapidly increased. The experimental RBE_{DSB} for the comparison in the high-LET region (closed diamonds ranging from 30 to 110 keV/μm in Fig. 4) were measured by plasmid DNA under dry conditions (*16*). As shown in Fig. 4, the PHITS simulation showed a similar tendency as that of the experimental RBE_{DSB} even in the high-LET region. For high-LET radiation, the DSB yields may be reduced by the release of fragments (*67*) (as well as multiple

DSBs (*68*)). In future development, it is needed to consider fragment release in this model.

Figure 5 shows the relationship between the RBE_{DSB} estimated by the PHITS code and the corresponding experimental values. In drawing this graph, the DSB yields for γ-rays (^{60}Co and ^{137}Cs sources), kVp X-rays (30–250 kVp), ultra-soft X-rays (Ti_K, Al_K, Cu_L, and C_K), monoenergetic electrons and monoenergetic protons were recalculated. Note that the experimental RBE_{DSB} values for electrons and photons were obtained from our previous paper (*32*). Thus, a reasonable recreation of the experimental behaviour was found ($R^2 = 0.748$). Note again that the experimental values for the high-LET protons were measured using dry DNA.

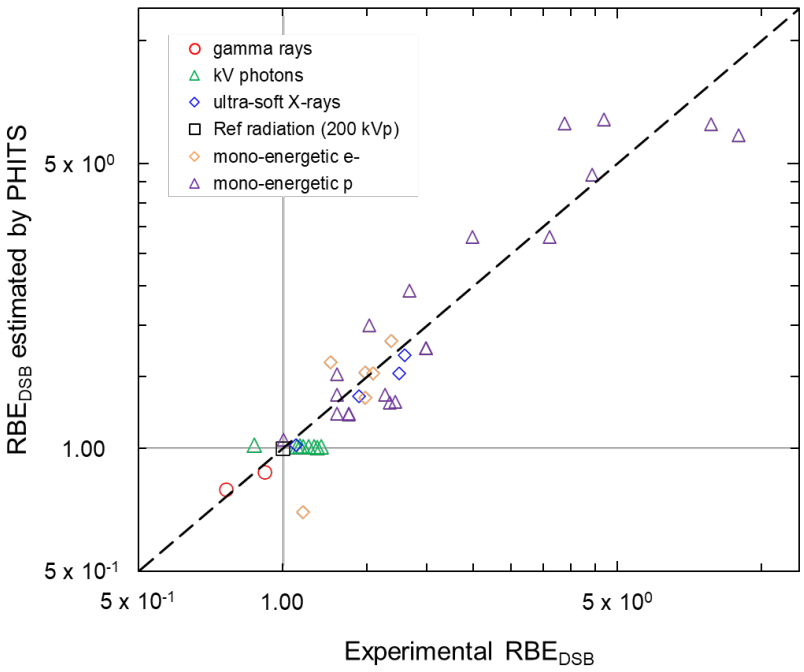

Figure 5. Comparison of the experimental RBE for DSB and the PHITS estimation. The reference radiation of the PHITS estimation is the 200-kVp X-rays with 0.5-mm Al and 0.5-mm Cu filtration. The RBE values calculated by PHITS are compared with the corresponding experimental values (*16*,*18*,*30*,*44*-*46*,*53*-*56*,*58*).

3-3. Depth dependence of RBE for PBT

According to the comparison of the DSB estimation by the PHITS and various available data in the literature, we then estimated the RBE_{DSB} value as a function of depth for the 60 MeV PBT. In this simulation, we considered the cell geometry. Figure 6A and 6B shows the examples of microscopic images of the fibroblast cells of WI-38 (shape and the stained nucleus) and the simple geometry, respectively.

Figure 6C shows the PDD of the 60 MeV protons, where the blue solid line and open circle are the simulated and measured PDD (*58*), respectively. The dose-averaged LET (noted as LET_d) is also depicted as a function of the depth. The red dashed line in Fig. 6D shows the depth dependence of RBE_{DSB} estimated by the *PHITS-KURBUC* mode using the cell geometry shown in Fig. S5A, which was compared with the experimental data of 53BP1 foci (*58*). The DSB yields were measured only at two positions: at a 1.38-mm depth for the entrance and a

31.5-mm depth for the Bragg peak. Focusing on the Bragg peak region, there is a subtle discrepancy between the PHITS simulation and the experimental data. Considering that the experimental uncertainties are shown as the standard error of the mean (s.e.m.), the inherent uncertainties of nuclear foci (standard deviation) are expected to be much higher than the s.e.m. Note that the standard deviations of the simulation results are less than 1%. In addition, the number of foci per nucleus dramatically changes at the Bragg peak region. Considering this, the uncertainty of placing a cell culture dish must be involved in the subtle difference. Meanwhile, the protein of 53BP1 at the DSB site involves binding to the phosphorylated histone H2AX (*69*) and regulating the repair balance between nonhomologous end joining and homologous recombination (*70*). The efficiency of detecting complex DSB yields by such biomarkers remains uncertain. Considering these, the overestimation by the simple model in the PHITS code is reasonable. Recently, a different model based on ion cluster size in the TOPAS-nBio (*31*) was proposed for directly using DNA damage estimation in the field of medical physics. To obtain better agreement with the experimental results, the methodology of the TOPAS-nBio will be useful for the future model development of the PHITS code.

As a preliminary study, the impact of the experimental geometry on DSB yield was also investigated by comparing to the benchmark results shown in Fig. 3. Using the cell geometry obtained from the DAPI staining of the cell nuclei, we estimated the LET dependence of the DSB yields. Figure S7A shows that the DSB yields calculated using the cell geometry (Fig. S5A) show a tendency similar to that in Fig. 3, which was calculated using the simple geometry in Fig. 1. From Fig. S7A, the yields considering the cell geometry for 750 keV protons are approximately 11% higher than those shown in Fig. 3 (benchmark data). This is due to the attenuation of proton energy when passing through cells. Meanwhile, we also considered a representative experimental geometry using plasmid DNA, where the plasmid DNA on the glass slide was surrounded by voids (Fig. S5B). As shown in Fig. S7B, the DSB yields for the plasmid DNA experiment are lower than those for the cell geometry in the low-LET region. This is because the secondary electron equilibrium does not hold for the plasmid DNA experiment. From these preliminary simulation results, we also confirmed that the PHITS code enables predicting DSB yields for various experimental conditions such as cultured cells and plasmid DNA in voids.

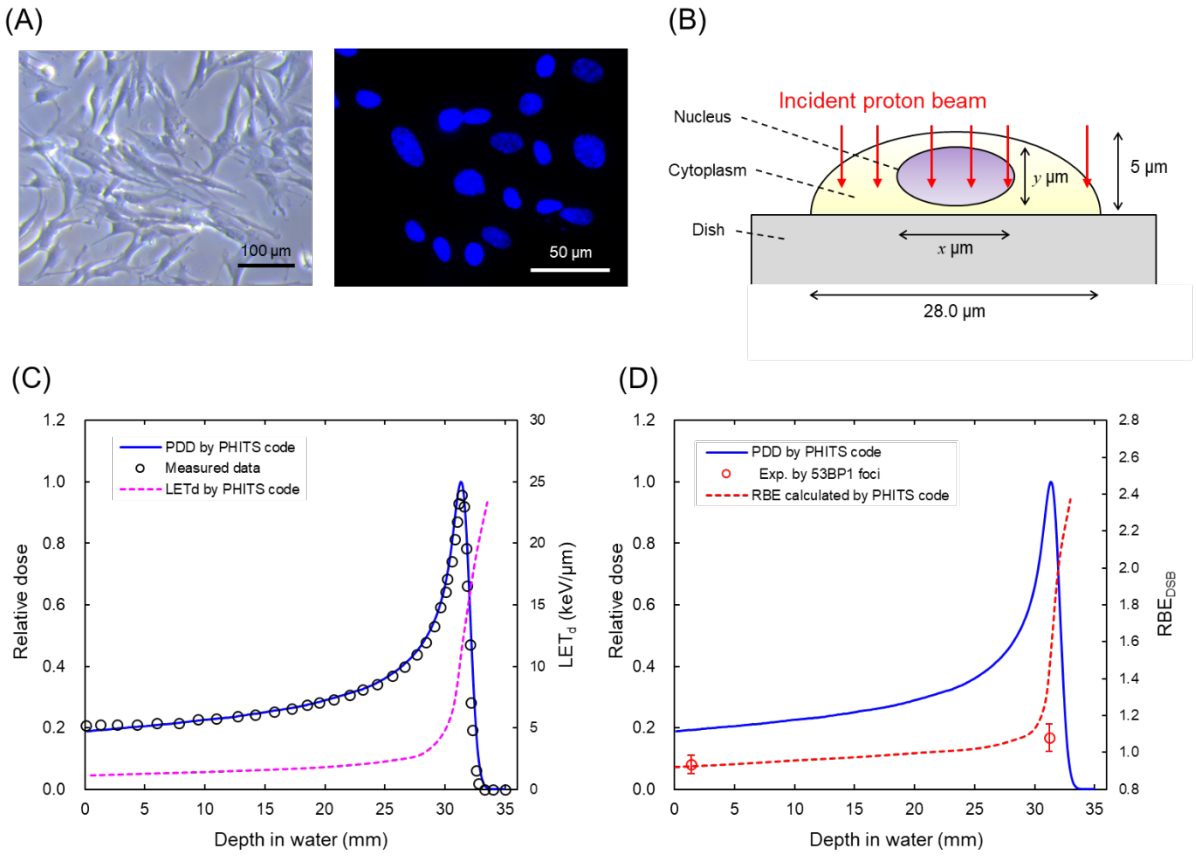

Figure 6. DSB estimation for the 60 MeV PBT. (A) shows an example of microscopic images and the cell nucleus of WI-38 stained by DAPI. (B) is the cell geometry considered in the PHITS code. (C) The PDD and LET of the 60 MeV PBT. (D) shows the depth dependence of RBE_{DSB} estimated by the *PHITS-KURBUC mode*. In Fig. 6B, we use the nucleus sizes for V79-379A (x = 11.0 μm, y = 3.89 μm) and WI-38 (x = 11.8 μm, y = 4.16 μm).

3-4. DSB complexity for electrons and protons

We finally estimated the yields of complex DSBs for 10 keV electrons, 30 MeV protons, 2.0 MeV protons, and 1.0 MeV protons. Figure 7 shows the content rates of sDSB, DSB+, and DSB++ estimated by the *PHITS-KURBUC mode*, which were compared with the other simulation results by KURBUC (*42*) and Geant4-DNA (*47*). There are differences between the individual Monte Carlo approaches in terms of relative or absolute differences. Considering this, we calculated the percentages of complex DSBs (DSB+ and DSB++) for comparison. As shown in Fig. 7, the contents of complex DSBs by the PHITS code show the tendencies similar to those of the other simulations in the case of low-LET radiation (10 keV e^-, 30 MeV $^1H^+$, and 2 MeV $^1H^+$). This may be because secondary electrons are major contributors to energy deposition. Meanwhile, focusing on the high-LET protons (1 MeV $^1H^+$), the PHITS code slightly overestimated the contents of complex DSBs in the same manner as that of the DSB yields (Fig. 3). The difference of the percentage between the PHITS code and other simulations are shown in Fig. S8, in which the difference for 1 MeV protons is the largest among 10 keV electrons, 30 MeV protons, 2.0 MeV protons, and 1.0 MeV protons. There is a possibility that

the other codes underestimated the amount of complex DSBs. However, considering the experimental data on DNA fragments released by high-LET ions, we should interpret that this is because the DNA damage estimation in PHITS does not consider the change in indirect DNA damage yields in relation to LET. Considering these, the LET dependence of indirect damage induced by chemical processes plays an important role in precisely understanding complex DSB induction after high-LET irradiation. In this regard, further development of a chemical model is needed in the future to reproduce the change of indirect damage induction. However, the present simple model implemented in PHITS is sufficient for estimating the yields for various DSB types for electrons and protons, as shown in Fig S9, showing the yields of sDSB, DSB+, and DSB++ for the 10 MeV electrons, 300 MeV protons, 100 MeV protons, 30 MeV protons, 10 MeV protons, and 3 MeV protons.

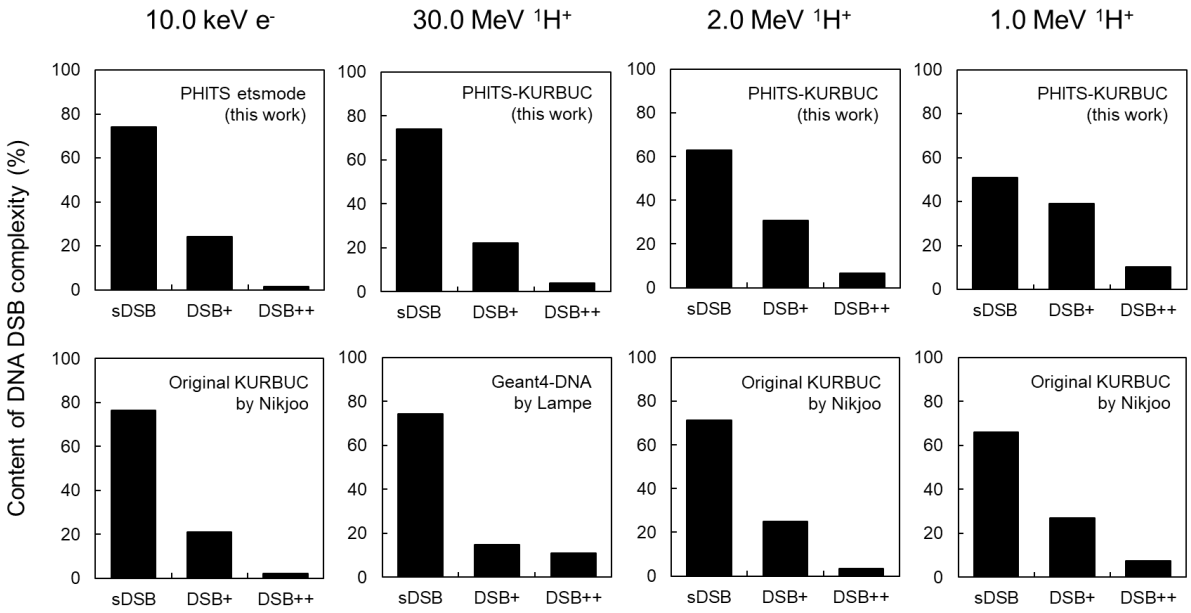

Figure 7. Estimation of DBS complexity (sDSB, DSB+, and DSB++). The upper histograms are the contents estimated by the *PHITS-KURBUC mode* (this work). The lower histograms are those estimated by KURBUC (*42*) and Geant4-DNA (*47*). The results of this work are calculated using the simple cluster analysis reported in a previous report (*34*).

4. CONCLUSION

In this study, we evaluated the yields of SSBs, DSBs, and complex DSBs for protons using the PHITS track-structure mode. The PHITS code was able to reproduce the experimental and simulated yields of various DNA lesion types for protons with low LET (less than about 30 keV/μm). From these comparisons, the current simplified DNA damage model is sufficient for estimating DNA lesion yields induced after protons with energies higher than 1 MeV (around the Bragg peak energy). Meanwhile, we found that the RBE for DSB depends on the experimental (irradiation) conditions in the case of high-LET protons, suggesting that further modellings of chemical processes and fragment releases are needed in future studies. In addition,

no experimental data on DSB yields for protons with energies lower than 1 MeV were available. The accumulation of such experimental yields for high-LET radiations (such as α particles (*71*)) is needed in the future.

A major aim of this work was to apply the DNA damage estimation model dedicated for electrons to simulations for proton beams. Meanwhile, our ultimate goal is to develop an all-in-one package for estimating radiobiological effects based on early DNA damage simulation and biophysical models. The present data on DSB yields would be useful as input information for biophysical models for predicting cell killing after irradiation, such as microdosimetric-kinetic (MK) model (*72*) and modified models (e.g., stochastic MK model (*73*,*74*) and integrated MK model (*75*,*76*)). This code for calculating DNA damage yields after the proton irradiation will be implemented in the PHITS package in the future. Further model developments such as the dependence of DNA damage induction on LET and new experimental data for high-LET particles in liquid water are essential for developing of DNA damage estimation model which can be directly used for medical field.

CONFLICT OF INTEREST

The authors declare that they have no conflict of interest.

FUNDING

This work was supported by the Japan Society for the Promotion of Science KAKENHI (Grant no. 19K17215, 22H03744), and was financially supported by the JAEA Fund for Exploratory Researches (Houga fund).

SUPPLEMENTARY MATERIALS

The following are available online:

- Figure S1: Benchmark test 1: DNA strand break yields for electrons,
- Figure S2: Benchmark test 2: DNA damage yields by photon irradiation and DBS complexity for electrons,
- Figure S3: Simulation geometry for photon beams,
- Figure S4: Measuring the size of cell nucleus,
- Figure S5: Simulation geometries for cell experiment and plasmid experiment,
- Figure S6: Benchmark test 3: DNA strand break yields for protons,
- Figure S7: Estimation of proton-induced DSB yields considering geometries for cell experiment and plasmid DNA experiment,
- Figure S8: Difference of complex DSB between PHITS and other simulations
- Figure S9: Estimation of yields of various DSB types for electrons and protons,
- Table S1: List of references for DNA damage yields by proton irradiations.

AUTHOR CONTRIBUTIONS

Y. Matsuya designed this study. A. Parisi and Y. Matsuya discussed the characteristics of proton particles and how to compare the simulation and the experimental data in literature. Y. Matsuya, T. Kai and Y. Yoshii developed the present model for estimating strand breaks yield. A. Parisi performed the calculations with the MCDS code. Y. Matsuya wrote the manuscript. T. Sato supervised this study. All authors reviewed the manuscript.

REFERENCES

[1] Levin, W.P., Kooy, H., Loeffler, J.S., DeLaney, T.F. Proton beam therapy. *Br. J. Cancer* 93, 849–854 (2005).

[2] Matsumoto, Y. Relative Biological Effectiveness and Fractionation of Proton-Beam Therapy. In: Tsuboi, K., Sakae, T., Gerelchuluun, A. (eds). Proton Beam Radiotherapy: Physics and Biology. 1st ed. Springer Nature Singapore Pte Ltd., 209–222 (2020).

[3] Date, H., Sutherland, K.L., Hayashi, T., Matsuzaki, Y., Kiyanagi, Y. Inelastic collision processes of low-energy protons in liquid water. *Radiat. Phys. Chem*. 75 179–187 (2006).

[4] Ödén, J., DeLuca, P.M., Orton, C.G. The Use of a Constant RBE=1.1 for Proton Radiotherapy Is No Longer Appropriate. *Med. Phys.* 45 (2), 502–505 (2018).

[5] Paganetti, H. Nuclear interactions in proton therapy: dose and relative biological effect distributions originating from primary and secondary particles. *Phys. Med. Biol.* 47 (5), p.747 (2002).

[6] Surova, O., Zhivotovsky, B. Various modes of cell death induced by DNA damage. Oncogene 32, 3789–3797 (2013).

[7] Olive PL. The role of DNA single- and double-strand breaks in cell killing by ionizing radiation. *Radiat. Res.* 150 (Suppl.), S42–S51 (1998).

[8] Carante MP, Altier S, Bortolussi S, Postuma I, Protti N, Ballarini F. Modeling radiation-induced cell death: role of different levels of DNA damage clustering. *Radiat. Environ. Biophys.* 54, 305–316 (2015).

[9] Ballarini F, Altieri S, Bortolussi S, Carante M, Giroletti E, Protti N. The BIANCA model/code of radiation-induced cell death: application to human cells exposed to different radiation types. *Radiat. Environ. Biophys.* 53, 525–533 (2014).

[10] Matsuya, Y., Sato, T., Nakamura, R., Naijo, S., Date, H. A theoretical cell-killing model to evaluate oxygen enhancement ratios at DNA damage and cell survival endpoints in radiation therapy. *Phys. Med. Biol.* 65, 095006 (2020).

[11] Paganetti, H. Significance and Implementation of RBE Variations in Proton Beam Therapy. Technol. Cancer Res. Treat. 2(5), 413-426 (2003).

[12] Mori, R., Matsuya, Y., Yoshii, Y., H. Date. Estimation of the radiation-induced DNA double-strand breaks number by considering cell cycle and absorbed dose per cell nucleus. *J. Radiat. Res*. 59(3), 253–260 (2018).

[13] D'Abrantes, S., Gratton, S., Reynolds, P., Kriechbaumer, V., McKenna, J., Barnard, S., Clarke, D.T., Botchway, S.W. Super-Resolution Nanoscopy Imaging Applied to DNA

552 Double-Strand Breaks. *Radiat. Res.* 189, 19–31 (2018).
553 [14] Ushigome, T., Shikazono, N., Fujii, K., Watanabe, R., Suzuki, M., Tsuruoka, C., Tauchi, H.,
554 Yokoya, A. Yield of Single- and Double-Strand Breaks and Nucleobase Lesions in Fully
555 Hydrated Plasmid DNA Films Irradiated with High-LET Charged Particles. *Radiat. Res.* 177,
556 614–627 (2012).
557 [15] Shiina, T., Watanabe, R., Shiraishi, I., Suzuki, M., Sugaya, Y., Fujii, K., Yokoya, A.
558 Induction of DNA damage, including abasic sites, in plasmid DNA by carbon ion and X-ray
559 irradiation. *Radiat. Environ. Biophys*. 52, 99–112 (2013).
560 [16] Souici, M., Khalil, T.T., Muller, D., Raffy, Q., Barillon, R., Belafrites, A., Champion, C.,
561 Fromm, M. Single- and Double-Strand Breaks of Dry DNA Exposed to Protons at Bragg-
562 Peak Energies. *J. Phys. Chem. B.* 121, 497–507 (2017).
563 [17] Tamborino, G., Perrot, Y., De Saint-Hubert, M., Struelens, L., Nonnekens, J., De Jong, M.,
564 Konijnenberg M.W., Villagrasa, C. Modeling Early Radiation DNA Damage Occurring
565 During 177Lu-DOTATATE Radionuclide Therapy. J. Nucl. Med. 63(5), 761–769 (2022).
566 [18] Vysin, L., Brabcova, K.P., Stepan, V., Moretto-Capelle, P., Bugler, B., Legube, G., Cafarelli,
567 P., Casta, R., Champeaux, J.P., Sence, M., Vlk, M., Wagner, R., Stursa, J., Zach, V., Incerti,
568 S., Juha, L., Davı´dkova´, M. Proton-induced direct and indirect damage of plasmid DNA.
569 *Radiat. Environ. Biophys.* 54, 343–352 (2015).
570 [19] Nikjoo, H., Goodhead, D.T., Charlton, D.E. and Paretzke, H.G. Energy deposition in small
571 cylindrical targets by monoenergetic electrons. *Int. J. Radiat. Biol.* 60, 739–756 (1991).
572 [20] Paretzke, H. G. Radiation track structure theory. In Kinetics of Nonhomogeneous Processes
573 (G. R. Freeman, Ed.), pp. 89–170. Wiley, New York (1987).
574 [21] Incerti, S. Baldacchino, G., Bernal, M., Capra, R., Champion, C., Francis, Z., Guatelli, S.,
575 Guèye, P., Mantero, A., Mascialino, B., Moretto, P., Nieminen, P., Rosenfeld, A., Villagrasa,
576 C., and Zacharatou, C. The Geant4-DNA project. *Int. J. Mod. Simul. Scien. Comput.* 01 (02),
577 157–178 (2010).
578 [22] Nikjoo, H., Emfietzoglou, D., Liamsuwan, T., Taleei, R., Liljequist, D., and Uehara, S.
579 Radiation track, DNA damage and response– a review. *Rep. Prog. Phys.* 79, 116601 (2016).
580 [23] Friedland, W., Dingfelder, M., Kundrát, P., and Jacob, P. Track structures, DNA targets and
581 radiation effects in the biophysical Monte Carlo simulation code PARTRAC. *Mutat. Res.*
582 711, 28 (2011).
583 [24] Yoshii, Y., Sasaki, K., Matsuya, Y., and Date, H. Cluster analysis for the probability of DSB
584 site induced by electron tracks. *Nucl. Instr. Methods Phys. Res. B.* 350, 55–59 (2015).
585 [25] Incerti, S., Kyriakou, I., Bordage, M.C., Guatelli, S., Ivanchenko, V., and Emfietzoglou, D.
586 Track structure simulations of proximity functions in liquid water using the Geant4-DNA
587 toolkit. *J. Appl. Phys.* 125, 104301 (2019).
588 [26] Xie, W., Li, J., Li, C., Qiu, R., Yan, C., Zeng, Z. Comparison of direct DNA strand break
589 simulated with different DNA models. *Radiat. Protect. Dosim*. 156(3), 283-288 (2013).
590 [27] Meylan, S., Incerti, S., Karamitros, M., Tang, N., Bueno, M., Clairand, I., Villagrasa, C.

591 Simulation of early DNA damage after the irradiation of a fibroblast cell nucleus using
592 Geant4-DNA. *Sci. Rep.* 7(1), 1–15 (2017).
593 [28] Nakano, H., Kawahara, D., Tanabe, S., Utsunomiya, S., Takizawa, T., Sakai, M., Nakano,
594 T., Ohta, A., Kaidu, M., Ishikawa, H. Calculated relative biological effectiveness (RBE) for
595 initial DNA double-strand breaks (DSB) from flattening filter and flattening filter-free 6 MV
596 X-ray fields. *BJR Open*. 3(1), 20200072 (2021).
597 [29] Saito, A., Kawahara, D., Nakano, H., Nagata, Y. DNA strand breaks based on Monte Carlo
598 simulation in and around the Lipiodol with flattening filter and flattening filter-free photon
599 beams. *Reports of Pract Oncol Radiother*. Ahead of print (2022), doi:
600 10.5603/RPOR.a2022.0067
601 [30] Francis, Z., Villagrasa, C., Clairand, I. Simulation of DNA damage clustering after proton
602 irradiation using an adapted DBSCAN algorithm. *Comput. Methods Programs. Biomed.*
603 101(3), 265–270 (2011).
604 [31] Ramos-Méndez, J., Burigo, L. N., Schulte, R., Chuang, C., Faddegon, B. Fast calculation of
605 nanodosimetric quantities in treatment planning of proton and ion therapy. Phys. Med. Biol.,
606 63(23), 235015 (2018).
607 [32] Matsuya, Y., Kai, T., Yoshii, Y., Yachi, Y., Naijo, S., Date, H., Sato, T. Modeling of yield
608 estimation for DNA strand breaks based on Monte Carlo simulations of electron track
609 structure in liquid water. *J. Appl. Phys.* 126, 124701 (2019).
610 [33] Matsuya, Y., Nakano, T., Kai, T., Shikazono, N., Akamatsu, K., Yoshii, Y., Sato, T. A
611 Simplified Cluster Analysis of Electron Track Structure for Estimating Complex DNA
612 Damage Yields. *Int. J. Mol. Sci.* 21, 1701 (2020).
613 [34] Matsuya, Y., Kai, T., Sato, T., Ogawa, T., Hirata, Y., Yoshii, Y., Parisi, A., Liamsuwan, T.
614 Track-structure mode in Particle and Heavy Ion Transport code System (PHITS): application
615 to radiobiological research. *Int. J. Radiat. Biol.* 98 (2), 148-157 (2022).
616 [35] Sato, T., Iwamoto, Y., Hashimoto, S., Ogawa, T., Furuta, T., Abe, S., Kai, T., Tsai, P-E.,
617 Matsuda, N., Iwase, H., Shigyo, N., Sihver, L., and Niita, K. Features of Particle and Heavy
618 Ion Transport code System (PHITS) version 3.02. *J. Nucl. Sci. Technol.* 55(5-6), 684–690
619 (2018).
620 [36] Matsuya, Y., Kai, T., Sato, T., Liamsuwan, T., Sasaki, K., Nikjoo, H. Verification of
621 KURBUC-based Ion Track Structure Mode for Proton and Carbon Ions in the PHITS Code.
622 *Phys. Med. Biol.* 66, 06NT02 (2021).
623 [37] Ogawa, T., Hirata, Y., Matsuya, Y., Kai, T. Development of proton track structure model
624 applicable to arbitrary materials. *Sci. Rep.* 11, 24401 (2021).
625 [38] Geissel, H., Scheidenberger, C., Malzacher, P., Kunzendorf, J., Weick, H., ATIMA,
626 Germany: GSI; http://web-docs.gsi.de/~weick/atima/ (accessed on May 2022)
627 [39] Hirayama, H., Namito, Y., Bielajew, A.F., Wilderman, S.J., Nelson, W.R. The EGS5 Code
628 System; Office of Scientific and Technical Information (OSTI): Oak Ridge, TN (2005).
629 [40] Ljungman, M., Nyberg, S., Nygren, J., Eriksson, M., Ahnstrom, G. DNA-bound proteins

630 contribute much more than soluble intracellular compounds to the intrinsic protection against
631 radiation-induced DNA strand breaks in human cells. *Radiat. Res.* 127, 171–176 (1991).
632 [41] Lobrich, M., Cooper, P.K., Rydberg, B. Non-random distribution of DNA double-strand
633 breaks induced by particle irradiation. *Int. J. Radiat. Biol.* 70, 493–503 (1996).
634 [42] Nikjoo, H., O'Neill, P., Wilson, W.E., Goodhead, D.T. Computational approach for
635 determining the spectrum of DNA damage induced by ionizing radiation. *Radiat. Res*. 156,
636 577–583 (2001).
637 [43] Friedland, W., Jacob, P., Bernhardt, Ph., Paretzke, H.G., Dingfelder, M. Simulation of DNA
638 damage after proton irradiation, *Radiat. Res.* 159, 401–410 (2003).
639 [44] Botchway, S.W., Stevens, D.L., Hill, M.A., Jenner, T.J., O'Neill, P. Induction and rejoining
640 of DNA double-strand breaks in chinese hamster V79-4 cells irradiated with characteristic
641 aluminum K and copper L ultrasoft X rays. *Radiat. Res.* 8, 317–324 (1997).
642 [45] Leloup, C., Garty, G., Assaf, G., Cristova, A., Breskin, A., Chechik, R., Shchemelinin, S.,
643 Paz-Elizur, T., Livneh, Z., Schulte, R.W., Bashkirov, V., Milligan, J.R., Grosswendt, B.
644 Evaluation of lesion clustering in irradiated plasmid DNA. *Int. J. Radiat. Biol.* 81(1), 41–54
645 (2005).
646 [46] Fulford, J., Nikjoo, H., Goodhead, D.T., O'Neill, P. Yields of SSB and DSB induced in DNA
647 by AlK ultrasoft X-rays and a-particles: comparison of experimental and simulated yields.
648 *Int. J. Radiat. Biol.* 77(10), 1053–1066 (2001).
649 [47] Lampe, N., Karamitros, M., Breton, V., Brown, J.M.C., Sakata, D., Sarramia, D., Incerti, S.
650 Mechanistic DNA Damage Simulations in Geant4-DNA Part 2: Electron and Proton Damage
651 in a Bacterial Cell. *Physica Medica* 48, 146–155 (2018).
652 [48] Ljungman, M., Nyberg, S., Nygren, J., Eriksson, M., Ahnström, G. DNA-Bound Proteins
653 Contribute Much More Than Soluble Intracellular Compounds to the Intrinsic Protection
654 against Radiation-Induced DNA Strand Breaks in Human Cells. *Radiat. Res.* 127 (2), 171–
655 176 (1991).
656 [49] Löbrich, M., Rydberg, B., Cooper, P.K. Repair of x-ray-induced DNA double-strand breaks
657 in specific Not I restriction fragments in human fibroblasts: joining of correct and incorrect
658 ends. *Proc. Natl. Acad. Sci. USA* 92, 12050–12054 (1995).
659 [50] Henthorn, N.T., Warmenhoven, J.W., Sotiropoulos, M., Aitkenhead, A.H., Smith, E.A.K.,
660 Ingram, S.P., Kirkby, N.F., Chadwick, A.L., Burnet, N.G., Mackay, R.I., Kirkbyab, K.J.,
661 Merchant, M.J. Clinically relevant nanodosimetric simulation of DNA damage complexity
662 from photons and protons. *RSC Adv.* 9, 6845–6858 (2019).
663 [51] Semenenko, V.A., Stewart, R.D. Fast Monte Carlo simulation of DNA damage formed by
664 electrons and light ions. *Phys. Med. Biol.* 51 (7), 1693–1706 (2006).
665 [52] Stewart, R.D. Yu, V.K., Georgakilas, A.G., Koumenis, C., Park, J.H., Carlson, D.J. Effects
666 of Radiation Quality and Oxygen on Clustered DNA Lesions and Cell Death. Radiat. Res.
667 176 (5), 587–602 (2011).
668 [53] Frankenberg, D., Brede, H.J., Schrewe, U.J., Steinmetz, C., Frankenberg-Schwager, M.,

669 Kasten, G., Pralle, E. Induction of DNA double strand breaks by 1H and 4He ions in primary
670 human skin fibroblasts in the LET range of 8 to 124 keV/mm. *Radiat. Res.* 151, 540–549
671 (1999).
672 [54] Belli, M., Cherubini, R., Vecchia, M.D., Dini, V., Moschini, G., Signoretti, C., Simone, G.,
673 Tabocchini, M.A., Tiveron, P. DNA DSB induction and rejoining in V79 cells irradiated with
674 light ions: a constant field gel electrophoresis study. *Int. J. Radiat. Biol*. 76 (8) 1095–1104
675 (2000).
676 [55] Belli, M., Cherubini, R., Vecchia, M.D., Dini, V., Esposito, G., Moschini, G., Sapora, O.,
677 Signoretti, C., Simone, G., Sorrentino, E., Tabocchini, M.A. DNA Fragmentation In
678 Mammalian Cells Exposed To Various Light Ions. *Adv. Space Res.* 27 (2) 393–399 (2001).
679 [56] Campa, A., Ballarini, F., Belli, M., Cherubini, R., Dini, V., Esposito, G., Friedland, W.,
680 Gerardi, S., Molinelli, S., Ottolenghi, A., Paretzke, H., Simone, G., Tabocchini, M.A. DNA
681 DSB induced in human cells by charged particles and gamma rays: Experimental results and
682 theoretical approaches. *Int. J. Radiat. Biol.* 81(11), 841–854 (2005).
683 [57] Antonelli, F., Belli, M., Cherubini, R., Dini, V., Esposito, G., Gerardi, S., Giardullo, P.,
684 Simone, G., Sorrentino, E., Tabocchini, M.A. DNA damage induced in human fibroblasts by
685 radiations of differing qualities. LNL annual report Appl. *Interdisciplinary Phys.* (2008).
686 https://www1.lnl.infn.it/~annrep/read_ar/2007/contributions/pdfs/051_B_32_B027.pdf
687 [58] Chaudhary, P., Marshall, T.I., Currell, F.J., Kacperek, A., Schettino, G., K.M. Prise.
688 Variations in the Processing of DNA Double-Strand Breaks Along 60-MeV Therapeutic
689 Proton Beams. *Int. J. Radiat. Oncol. Biol. Phys.* 95(1) 86e94 (2016).
690 [59] Okamoto, H., Kanai, T., Kase, Y. et al. Relation between lineal energy distribution and
691 relative biological effectiveness for photon beams according to the microdosimetric kinetic
692 model. *J. Radiat. Res.* 52, 75–81 (2011).
693 [60] ICRU report 49. International Commission on Radiation Units and Measurements, Maryland,
694 USA: Bethesda (1993).
695 [61] Friedland, W., Schmitt, E., Kundrát, P., Dingfelder, M., Baiocco, G., Barbieri, S., Ottolenghi,
696 A. Comprehensive track-structure based evaluation of DNA damage by light ions from
697 radiotherapyrelevant energies down to stopping. *Sci. Rep.* 7, 45161 (2017).
698 [62] Emfietzoglou, D., Garcia-Molina, R., Kyriakou, I., Abri,l I., Nikjoo, H. A dielectric response
699 study of the electronic stopping power of liquid water for energetic protons and a new I-value
700 for water. *Phys. Med. Biol*. 54, 3451–3472 (2009).
701 [63] Francis, Z., Incerti, S., Karamitros, M., Tran, H.N., Villagrasa, C. Stopping power and ranges
702 of electrons, protons and alpha particles in liquid water using the Geant4-DNA package. *Nucl.
703 Instr. Methods Phys. Res. B* 269, 2307–2311 (2011).
704 [64] Rasband, W. S., ImageJ, U. S. National Institutes of Health, Bethesda, Maryland, USA,
705 http://imagej.nih.gov/ij/ (1997–2012).
706 [65] Sakata, D., Suzuki, M., Hirayama, R., Abe, Y., Muramatsu, M., Sato, S., Belov, O., Kyriakou,
707 I., Emfietzoglou, D., Guatelli, S., Incerti, S., Inaniwa, T. Performance Evaluation for Repair

of HSGc-C5 Carcinoma Cell Using Geant4-DNA. *Cancers* 13, 6046 (2021).

[66] Shin, W-G., Sakata, D., Lampe, N., Belov, P., Tran, N.H., Petrovic, I., Ristic-Fira, A., Dordevic, M., Bernal, M.A., Bordage, M-C., Francis, Z., Kyriakou, I., Perrot, Y., Sasaki, T., Villagrasa, C., Guatelli, S., Breton, V., Emfietzoglou, D., Incerti, S. A Geant4-DNA Evaluation of Radiation-Induced DNA Damage on a Human Fibroblast. *Cancers*. 13, 4940 (2021).

[67] Friedland, W., Jacob, P., Paretzke, H.G., Ottolenghi, A., Ballarini, F,, Liotta, M. Simulation of light ion induced DNA damage patterns. *Radiat. Prot. Dosim.* 122(1-4), 116–120 (2006).

[68] Hunniford, C.A., McCullough, R.W., Davies, R.J.H., Timson, D.J. DNA damage by low-energy ions. *Biochem. Soci. Trans.* 37(4), 893–896 (2009).

[69] Ward, I.M., Minn, K., Jorda, K.G., Chen, J. Accumulation of Checkpoint Protein 53BP1 at DNA Breaks Involves Its Binding to Phosphorylated Histone H2AX. *J. Biol. Chem.* 278 (22) 19579–19582 (2003).

[70] Guo, X., Bai, Y., Zhao, M., Zhou, M., Shen, Q., Yun, C.H., Zhang, H., Zhu, W.G., Wang, J. Acetylation of 53BP1 dictates the DNA double strand break repair pathway. *Nucleic Acids Res.* 46(2), 689–703 (2018).

[71] Nikitaki, Z., Nikolov, V., Mavragani, I.V. Mladenov, E., Mangelis, A., Laskaratou, D.A., Fragkoulis, G.I., Hellweg, C.E., Martin, O.A., Emfietzoglou, D., Hatzi, V.I., Terzoudi, G.I., Iliakis, G., Georgakilas, A.G. Measurement of complex DNA damage induction and repair in human cellular systems after exposure to ionizing radiations of varying linear energy transfer (LET). Free Radical Res. 50 (Sup1), S64–S78 (2016).

[72] Hawkins, R.B. A statistical theory of cell killing by radiation of varying linear energy transfer. *Radiat. Res.* 140, 366–374 (1994).

[73] Sato, T., Furusawa, Y. Cell Survival Fraction Estimation Based on the Probability Densities of Domain and Cell Nucleus Specific Energies Using Improved Microdosimetric Kinetic Models. *Radiat. Res.* 178(4):341–356 (2012).

[74] Sato, T., Hashimoto, H., Inaniwa, T., Takada, K., Kumada, H. Implementation of simplified stochastic microdosimetric kinetic models into PHITS for application to radiation treatment planning. *Int. J. Radiat. Res*. 97(10), 1450–1460 (2021).

[75] Matsuya, Y., Sasaki, K., Yoshii, Y., Okuyama, G., Date, H. Integrated Modelling of Cell Responses after Irradiation for DNA-Targeted Effects and Non-Targeted Effects. *Sci. Rep.* 8, 4849 (2018)

[76] Matsuya, Y., McMahon, S.J., Ghita, M., Yoshii, Y., Sato, T., Date, H., Prise, K.M. Intensity Modulated Radiation Fields Induce Protective Effects and Reduce Importance of Dose-Rate Effects. *Sci. Rep.* 9, 9483 (2019).